# EFFECTS OF FORMATION STRESS ON LOGGING MEASUREMENTS

Xiaojun Huang, Zhenya Zhu, M. Nafi Toksöz, and Daniel R. Burns

Earth Resources Laboratory
Department of Earth, Atmospheric, and Planetary Sciences
Massachusetts Institute of Technology
Cambridge, MA 02139

## ABSTRACT

We show both theoretically and experimentally how stress concentrations affect the velocity field around a borehole surrounded by a formation with intrinsic ortohombic anisotropy. When $F_x = F_y$, no extra anisotropy is induced, however, isotropic stress concentrations are developed in the neighborhood of the borehole. Extra anisotropy is induced only when $F_x \neq F_y$, and the level of induced anisotropy is affected by the intrinsic anisotropy of the formation. Experiments show that monopole acoustic waves are more sensitive to properties in the neighborbood of the borehole than dipole waves. However, only dipole logging can determine the direction of anisotropy. A combination of monopole and dipole logging may lead to a better investigation of intrinsic as well as induced anisotropy of the formation.

## INTRODUCTION

The elastic velocity of a small-amplitude wave is affected by formation stresses or pre-stresses presumably caused by tectonics and overburden. Traditionally, this phenomenon has been modeled using distributions of microcracks (Eshelby, 1957; Anderson *et al.*, 1974). In recent years, laboratory experiments show that the theory of acoustoelasticity can be used to model stress-induced velocity changes in formations or rocks (Winkler and Liu, 1996; Winkler *et al.*, 1998). The theory of acoustoelasticity, originally developed in the context of thermoelasticity (Toupin and Bernstein, 1961; Thurston and Brugger, 1964; Sinha, 1982; Pao and Gamer, 1985), is based on the approach of a small dynamic field superimposed on a static deformation. The pre-stress is thought to change the effective elasticity of a medium. Accordingly, the anisotropic property

and elastic velocities of the medium will change. Researchers have applied the theory of acoustoelasticity to study the influence of pre-stresses on elastic waves propagating along a fluid-filled borehole (Norris *et al.*, 1994; Sinha and Kostek, 1996; Liu and Sinha, 2000). It has been proven both numerically and experimentally that a crossover in flexural dispersions is an indicator of stress-induced anisotropy. Crossover in flexural dispersions has been observed in field data. Using a multi-frequency inversion technique, Huang and Sinha (1999) estimated formation stresses using sonic logging data. Using a phenomenological stress-velocity coupling relation, Tang *et al.* (1999) developed a theory to explain shear-wave splitting observed in field monopole logging data. A further derivation shows Tang's approach agrees with the theory of acoustoelasticity.

A common assumption is that the formation is isotropic, but a good number of underground rocks exhibit considerable intrinsic anisotropy. In this paper, we present a theoretical framework for wave propagation along a fluid-filled borehole surrounded by a pre-stressed formation with intrinsically orthohombic anisotropy. Analytical results show that the existence of a borehole always causes heterogeneous velocity field distribution in the vicinity of a borehole subject to far field stresses. When far-field biaxially stresses $F_x$ and $F_y$ are not balanced, i.e., $F_x \neq F_y$, extra anisotropy is induced to the formation which can be detected by both dipole and monopole tools. When $F_x \neq F_y$, no extra anisotropy will be induced, but velocities in the formation are generally higher than without stresses. Theoretical results are validated by a repeatable laboratory experiment consisting of measuring the intrinsic anisotropy of a granite rock and the anisotropy induced by the stresses perpendicular to the borehole axis. Four nonlinear elastic constants were inverted from shear velocity measurements based on theoretical expressions for formation shear velocities as functions of the magnitude of uniaxial stresses. Our experiments also show that shear head waves received by monopoles are more sensitive to formation stress variation than flexural waves received by dipole receivers.

## EFFECTS OF FORMATION STRESSES ON VELOCITY FIELD AROUND A BOREHOLE: THEORY

Consider a borehole surrounded by an originally homogeneous solid with orthohombic anisotropy where the solid formation is subject to biaxial stresses, $F_x$ and $F_y$, in the $x$- and $y$-directions in the far field (Figure 1). The compressive biaxial stresses are presumably caused by plate tectonics. The existence of a borehole leads to stress concentration near the borehole. The stress distribution in the vicinity of a borehole is

given by Timoshenko and Goodier (1982)

$$\begin{aligned} T_{rr} &= F^+(1-\frac{a^2}{r^2}) + F^-(1+\frac{3a^4}{r^4}-\frac{4a^2}{r^2})\cos 2\theta\,, \\ T_{\theta\theta} &= F^+(1+\frac{a^2}{r^2}) - F^-(1+\frac{3a^4}{r^4})\cos 2\theta\,, \\ T_{r\theta} &= F^-(1-\frac{3a^4}{r^4}+\frac{2a^2}{r^2})\sin 2\theta\,, \\ T_{zr} &= 0\,, \\ T_{z\theta} &= 0, \end{aligned} \tag{1}$$

where $F^+ = \frac{F_x+F_y}{2}$ and $F^- = \frac{F_x-F_y}{2}$, and $a$ denotes the radius of the borehole. Figure 2 shows the static stress concentration around the borehole induced by a compressional uniaxial stress $F_x$. In the neighbourhood of the borehole, $T_{rr}$ and $T_{\theta\theta}$ developed compressional concentration in the $y$ direction and tensile stress concentration in the $x$ direction, whereas stress concentration of $T_{zz}$ and $T_{r\theta}$ are $90^o$ and $45^o$ different, respectively. Stress concentrations happen even when $F_x = F_y$ in the far field (Figure 3). If we denote static displacements caused by the aforementioned formation stresses in $r$, $\theta$, and $z$ directions as $w_r$, $w_\theta$, and $w_z$, respectively, the corresponding static strains in the formation are

$$\begin{aligned} E_{rr} &= \frac{\partial w_r}{\partial r}\,, \\ E_{\theta\theta} &= \frac{w_r}{r} + \frac{1}{r}\frac{\partial w_\theta}{\partial \theta}\,, \\ E_{zz} &= \frac{\partial w_z}{\partial z}\,, \\ E_{\theta z} &= \frac{\partial w_\theta}{\partial z} + \frac{1}{r}\frac{\partial w_z}{\partial \theta}\,, \\ E_{rz} &= \frac{\partial w_r}{\partial z} + \frac{\partial w_z}{\partial r}\,, \\ E_{r\theta} &= \frac{1}{r}\frac{\partial w_r}{\partial \theta} + \frac{\partial w_\theta}{\partial r} - \frac{1}{r}w_\theta. \end{aligned} \tag{2}$$

Because the borehole is very long in the axial or $z$-direction, the biaxial stresses are perpendicular to axial direction and do not vary in the region of interest. It is reasonable to assume that all cross sections are in the same condition and there is no displacement in the axial direction. $w_z$, $E_{zz}$, $E_{zr}$, $E_{z\theta}$, $T_{zr}$, and $T_{z\theta}$ vanish as a result. According to the theory of acoustoelasticity, the relationship of the static stress and strain complies with Hooke's Law. There are nine independent linear elastic constants for orthohombic anisotropic solids: $c_{11}$, $c_{12}$, $c_{13}$, $c_{22}$, $c_{23}$, $c_{33}$, $c_{44}$, $c_{55}$, and $c_{66}$. The normal stress in the axial direction $T_{zz}$ is therefore

$$T_{zz} = c_{13}E_{rr} + c_{23}E_{\theta\theta} \tag{3}$$

where

$$E_{rr} = \frac{c_{12}T_{\theta\theta} - c_{22}T_{rr}}{A}, \tag{4}$$

$$E_{\theta\theta} = \frac{c_{12}T_{rr} - c_{11}T_{\theta\theta}}{A} \tag{5}$$

and

$$A = c_{12}^2 - c_{11}c_{22l}\,.$$

Static displacements are obtained by integration of equations (4) and (5),

$$\begin{aligned} w_r &= \frac{c_{12}}{A}\left[F^+(r - \frac{a^2}{r}) - F^-(r - \frac{a^4}{r^3})\cos 2\theta\right] \\ &- \frac{c_{22}}{A}\left[F^+(r + \frac{a^2}{r} - 2a) + F^-(r - \frac{a^4}{r^3} + \frac{4a^2}{r} - 4a)\cos 2\theta\right] \end{aligned} \tag{6}$$

$$\begin{aligned} w_\theta &= \frac{c_{12}}{A}F^-(r + \frac{a^4}{r^3} - \frac{2a^2}{r})\sin 2\theta \\ &+ \frac{c_{22}}{A}\left[F^+(r + \frac{a^2}{r} - 2a)\theta + \frac{F^-}{2}(r - \frac{a^4}{r^3} + \frac{4a^2}{r} - 4a)\sin 2\theta\right] \\ &- \frac{c_{11}}{A}\left[F^+(r + \frac{a^2}{r})\theta - \frac{F^-}{2}(r + \frac{3a^4}{r^3})\sin 2\theta\right]. \end{aligned} \tag{7}$$

Since it is more convenient to work in Cartesian coordinates later on, we convert static stresses and displacements to Cartesian coordinates by rotating them by $-\theta$, and convert $\theta$ and $\rho$ into $tan^{-1}(y/x)$ and $\sqrt{x^2+y^2}$, respectively, i.e.,

$$T_{xx} = \frac{x^2}{x^2+y^2}T_{rr} + \frac{y^2}{x^2+y^2}T_{\theta\theta} - \frac{2xy}{x^2+y^2}T_{r\theta}\,, \tag{8}$$

$$T_{yy} = \frac{y^2}{x^2+y^2}T_{rr} + \frac{x^2}{x^2+y^2}T_{\theta\theta} + \frac{2xy}{x^2+y^2}T_{r\theta}\,, \tag{9}$$

$$T_{xy} = \frac{xy}{x^2+y^2}(T_{rr} - T_{\theta\theta}) + \frac{x^2-y^2}{x^2+y^2}T_{r\theta}\,, \tag{10}$$

$$T_{xz} = T_{yz} = 0\,, \tag{11}$$

$$w_x = w_r\frac{x}{\sqrt{x^2+y^2}} - w_\theta\frac{y}{\sqrt{x^2+y^2}}\,, \tag{12}$$

$$w_y = w_r\frac{y}{\sqrt{x^2+y^2}} + w_\theta\frac{x}{\sqrt{x^2+y^2}}\,, \tag{13}$$

$$w_z = 0\,. \tag{14}$$

## Formation Stress on Logging Measurements

In the presence of biaxial stresses in the propagating medium, equations of motion describing small-amplitude waves are written in terms of the modified Piola-Kirchhoff stress tensor of first-line $\tau_{\alpha j}$. Introducing Piola-Kirchhoff stresses is necessary in a nonlinear formulation that accounts for changes in the surface area and surface normal caused by a finite deformation of the material. Referring to the statically deformed (intermediate) configuration, the equation of motion and constitutive relation of small-amplitude wave propagating in a pre-stressed medium are (Norris *et al.*, 1994)

$$\rho v_{j,t} = \tau_{\alpha j,\alpha} \tag{15}$$

and

$$\tau_{\alpha j,t} = (c_{\alpha j\gamma\beta} + H_{\alpha j\gamma\beta}) v_{\beta,\gamma}\,, \tag{16}$$

where $\rho$ is the formation density in the intermediate state, and $c_{\alpha j\gamma\beta}$ represents the second-order elastic constant. We comply with the convention that a comma followed by an index $\alpha$ or $t$, denotes differentiation with respect to the corresponding axis or time, respectively. Both the lower case Latin and Greek letters take on the values 1, 2, and 3, corresponding to the $x$, $y$ and $z$ directions, respectively. The Einstein summation convention for repeated tensor indices is also implied. Using $c_{\alpha j\gamma\beta AB}$ to denote the third-order elastic constant, the effective elastic stiffness tensor $H_{\alpha j\gamma\beta}$ can be written as

$$H_{\alpha j\gamma\beta} = g_{\alpha j\gamma\beta} + T_{\alpha\gamma}\delta_{j\beta} + P_0(\delta_{\alpha j}\delta_{\gamma\beta} - \delta_{\alpha\gamma}\delta_{j\beta})\,, \tag{17}$$

where $P_0$ is the hydrostatic pressure in a borehole which we have set equal to zero, as there is no water in the borehole in later experiment, and

$$\begin{aligned} g_{\alpha j\gamma\beta} &= -c_{\alpha j\gamma\beta} w_{\eta,\eta} + c_{\alpha j\gamma\beta AB} E_{AB} + w_{\alpha,L} c_{Lj\gamma\beta} \\ &+ w_{j,M} c_{\alpha M\gamma\beta} + w_{\gamma,P} c_{\alpha jP\beta} + w_{\beta,Q} c_{\alpha j\gamma Q}\,, \end{aligned} \tag{18}$$

and $T_{\alpha\gamma}$ and $E_{AB}$ are the static stress and strain in the formation given by

$$T_{\alpha\gamma} = c_{\alpha\gamma\beta\delta} w_{\delta,\beta}\,, \tag{19}$$

and

$$E_{AB} = \frac{1}{2}(w_{A,B} + w_{B,A})\,. \tag{20}$$

We next derive expressions for plan-wave speeds in terms of static stress field. The resulting expressions for the compressional and shear wave velocities for wave propagating along the $z-$direction in a medium with orthohombic anisotropy subject to biaxial stress field $F_x$ and $F_y$ in the far-field are given by

$$\begin{aligned} \rho V_P^2(x,y) &= c_{33} + \frac{c_{133} - c_{33}}{A}(c_{12}T_{yy} - c_{22}T_{xx}) + \frac{c_{233} - c_{33}}{A}(c_{12}T_{xx} - c_{11}T_{yy}) \\ &+ \frac{c_{13}}{A}(c_{12}T_{yy} - c_{22}T_{xx}) + \frac{c_{23}}{A}(c_{12}T_{xx} - c_{11}T_{yy})\,, \end{aligned} \tag{21}$$

$$\rho V_{S_x}^2(x,y) = c_{55} + \frac{c_{155}+c_{55}}{A}(c_{12}T_{yy} - c_{22}T_{xx}) + \frac{c_{255}-c_{55}}{A}(c_{12}T_{xx} - c_{11}T_{yy}) + \frac{c_{13}}{A}(c_{12}T_{yy} - c_{22}T_{xx}) + \frac{c_{23}}{A}(c_{12}T_{xx} - c_{11}T_{yy}) \quad (22)$$

and

$$\rho V_{S_y}^2(x,y) = c_{44} + \frac{c_{144}-c_{44}}{A}(c_{12}T_{yy} - c_{22}T_{xx}) + \frac{c_{244}+c_{44}}{A}(c_{12}T_{xx} - c_{11}T_{yy}) + \frac{c_{13}}{A}(c_{12}T_{yy} - c_{22}T_{xx}) + \frac{c_{23}}{A}(c_{12}T_{xx} - c_{11}T_{yy}). \quad (23)$$

Substituting properties of an isotropic dry Berea Sandstone block measured by Winkler *et al.* (1988), equations (21), (22) and (23) yield velocity predictions that are differ within 5%. Velocity fields in the formation subject to compressional uniaxial stress $F_x = -1MPa$, $F_x = -3MPa$, biaxial stress $F_x = F_y = -1MPa$, $F_x = F_y = -3MPa$ and $F_x = -4MPaF_y = -1MPa$ are shown in Figures 4, 5, 6, 7, and 8, respectively. Conclusions drawn from the figures are: (1) The velocity field in the originally homogeneous formation becomes heterogeneous when the formation is subject to stresses even when $F_x = F_y$ in the far field; (2) when $F_x \neq F_y$, extra anisotropy is induced by stresses, and is much stronger in the vicinity of the borehole. Stress-induced anisotropy can be detected, together with intrinsic anisotropy in the form of flexural wave splitting in dipole logging or shear head wave splitting in monopole logging; and (3) no extra anisotropy is induced when $F_x = F_y$.

## BOREHOLE MODEL AND MEASUREMENTS

Figure 1 shows a granite borehole model of 20 cm × 10 cm × 10 cm. A hole of 1.1 cm in diameter is drilled along the long axis (Z axis). To illustrate the induced heterogeneity of the effective elastic stiffness of the rock resulting from stress concentration around the borehole, we selected three locations—A, B, and C—to measure the P- and S-velocities. Locations A and B are close to the borehole and are in X and Y directions, respectively. For each location, a P-wave and two shear wave velocities are measured without applying any stresses. The velocities of the shear wave with polarization at the X axis and at the Y axis are about 2400 m/s and 2700 m/s, respectively. They are a little higher at locations A and B, where they are close to the borehole, indicating the existence of residual stresses during dilling. There are about 10% intrinsic anisotropy (Figure 1). The diameter of the plane transducers used in our measurements is 1.27 cm. The velocities measured at locations A and B are point values due to the size of the transducers.

### Effect of Stress on Borehole Anisotropy

We investigate the effects of a uniaxial stress perpendicular to the borehole axis on the rock anisotropy by measuring the shear velocities at locations A, B, and C when a stress

is applied in the X- or Y-direction. The properties of the rock are listed in Table 1. Figure 9 shows the shear velocities with different polarization and at the three locations when the uniaxial stress is in X-direction (Figure 9a) or at the Y-direction (Figure 9b). All velocities increase when the applied stress increases. When the stress is in the X-direction (the polarization direction of the slow shear wave), the increase of slow shear velocities is higher than that of fast shear velocities at the three measurement locations. If the stress is at the Y-direction (the polarization direction of the fast shear wave), the increase of the slow shear velocity is higher than the fast one at location B, but is lower than the fast one at location A and C. This phenomenon could be attributed to rock heterogeneity, either intrinsic or caused by drilling. The stress at the Y-direction does not change the ratio between fast and slow shear velocities at location C very much. This shows that the stress-induced anisotropy is stronger around the borehole, which is consistent with theoretical predications. Equations (22) and (23) show that $\rho V_{S_x}^2$ and $\rho V_{S_y}^2$ are linear functions of uniaxial stress magnitude $F_x$ or $F_y$, and slopes of $\rho V_{S_x}^2$ and $\rho V_{S_y}^2$ with respect to uniaxial stress magnitude are functions of third-order nonlinear elastic constants $c_{155}$, $c_{255}$ and $c_{144}$, $c_{244}$, respectively. As a result, these nonlinear elastic constants can be estimated from laboratory measurements (Table 2).

| $\rho$ ($kg/m^3$) | $c_{11}$ (GPa) | $c_{12}$ (GPa) | $c_{13}$ (GPa) | $c_{22}$ (GPa) | $c_{23}$ (GPa) | $c_{33}$ (GPa) | $c_{44}$ (GPa) | $c_{55}$ (GPa) | $c_{66}$ (GPa) |
|---|---|---|---|---|---|---|---|---|---|
| 2660 | 32.96 | −2.50 | 0.70 | 41.92 | −0.35 | 50.10 | 19.78 | 16.12 | 16.36 |

Table 1: Material properties of the granite.

| $c_{155}$ (GPa) | $c_{255}$ (GPa) | $c_{144}$ (GPa) | $c_{244}$ (GPa) |
|---|---|---|---|
| −9030 | 24874 | 25882 | −15864 |

Table 2: Nonlinear elastic constants inverted from $V_{S_x}^A$,$V_{S_x}^B$,$V_{S_y}^A$ and $V_{S_y}^B$.

## Logging Measurement in the Borehole

We performed experiments to measure the monopole and dipole responses in a stressed borehole. The setup is shown schematically in Figure 10a. A pair of transducers with 0.9 cm in diameter is applied to generate and receive the monopole or dipole waves in the borehole. The transducers can be connected as monopole or dipole transducers with a switch (Zhu *et al.*, 1994) One transducer is mounted at a lower section of the borehole and excited by an electric pulse. The other one moves step by step along the borehole and records the acoustic waves propagating along the borehole. Figure 10b shows a typical record of the acoustic waveforms when a stress of 5 MPa is at the X-direction.

From the waveforms we can see the P-wave, shear waves and Stoneley wave with high amplitude. We can calculate the velocity for each wave from its slope. In the record shown in Figure 10b, the sampling rate is 0.2 $\mu$s. When we decrease the sampling rate to 0.1 $\mu$s, velocities can be calculated more accurately. There are two shear waves at their arriving area with different velocity. When the stress is in the X- or Y-direction, we record the monopole waveforms and calculate the velocities of the two shear waves. Because the monopole transducer is symmetric with no polarization in the horizontal plane, the directions of the anisotropy induced by stress can not be determined from the monopole waveforms.

Figure 11 shows the relationship between stress and shear wave velocities when the stress is in the X-direction (Figure 11a) or the Y-direction (Figure 11b), and varies from 0 to 6 MPa. The shear velocities measured in the borehole without a stress are different from those measured on the rock block (Figure 1). The fast shear velocity of 2680 m/s measured in the borehole is lower than the velocity (2700 m/s or 2760 m/s) measured on the rock block in Figure 1. On the other hand, the slow shear velocity of 2540 m/s measured in the borehole is obviously higher than the velocity of 2450 m/s or 2490 m/s measured on the rock block. Theses results may be caused by intrinsic heterogeneity of the rock and/or residual stresses induced by drilling. Figure 11 shows the variation of fast and slow shear waves with the stress perpendicular to the borehole axis. The fast shear velocity increases and the slow shear velocity decreases when the stress increases. This is consistent with our theoretical predictions. According to the theory, compressional stress concentrations develop in the direction perpendicular to the uniaxial stress direction, and tensile stress concentrations develop in the stress direction (Figure 2). Therefore, the slow shear wave is polarized in the same direction as the uniaxial stress direction, and the fast shear wave is polarized in the perpendicular direction. Furthermore, equations (2), (22) and (23) show that the fast shear velocity increases while the slow shear velocity decreases with respect to uniaxial stress. In particular, it is clearly shown in the experiment that, when the stress is at the Y-direction, the polarization direction of the fast shear wave, the stress induces stronger anisotropy on the borehole wall.

## CONCLUSIONS

Far-field stresses in a plane perpendicular to a borehole axis will induce stress concentrations near the borehole, whether or not $F_x = F_y$. As a result, the heterogeneous shear wave velocity field is always developed in the vicinity of a borehole. When $F_x = F_y$, no extra anisotropy is induced despite the intrinsic elastic property of the formation. On the other hand, extra anisotropy is induced only when $F_x \neq F_y$, and the level of induced anisotropy is affected by the intrinsic anisotropy of the formation. Our experiment also shows that monopole acoustic waves are more sensitive to properties in the neighborhood of the borehole than dipole waves, however, only dipole logging can determine the direction of anisotropy. A combination of monopole and dipole logging may lead to

better investigation of the intrinsic as well as the induced anisotropy of the formation.

## ACKNOWLEDGMENTS

This work was supported by the Borehole Acoustics and Logging/Reservoir Delineation Consortia at the Massachusetts Institute of Technology.

## REFERENCES

Anderson, D.L., Minster, B., and Cole, D., 1974, The effect of oriented cracks on seismic velocities, *J. Geophys. Res., 79,* 4011–4105.

Eshelby, J., 1957, The determination of the elastic field of an ellipsoidal inclusion and related problems, *Proc. Roy. Soc., Ser. A., 241,* 376–396.

Huang, X. and Sinha, B.K., 1999, Formation stress determination from borehole acoustic logging: A theoretical foundation, *Expanded Abstracts, Soc. Explor. Geophys., BG2.7,* 57–60.

Liu, Q.-H. and Sinha, B.K., 2000, Multiple acoustic waveforms in fluid-filled boreholes in biaxially stressed formation: A finite-difference method, *Geophysics, 100,* 1392–1398.

Norris, A.N., Bikash, K.S., and Kostek, S., 1994, Acoustoelasticity of solid/fluid composite systems, *Geophys. J. Int., 118,* 439–446.

Pao, Y.-H. and Gammer, U., 1985, Acoustoelastic waves in orthotropic media, *J. Acoust. Soc. Am., 77,* 806–812.

Sinha, B., 1982, Elastic waves in crystals under a bias, *Ferroelectrics, 41,* 61–73.

Sinha, B.K. and Kostek, S., 1996, Stress-induced azimuthal anisotropy in borehole flexural waves, *Geophysics, 61,* 1899–1907.

Tang, X., 1999, Formation stress determination from borehole acoustic logging: A theoretical foundation, *Expanded Abstracts, Soc. Explor. Geophys., BG27.7,* 57–60.

Thurston, R.N. and Brugger, K., 1964, Third-order elastic constants and the velocity of small amplitude elastic waves in homogeneously stressed media, *Phys. Rev., 33,* A1604–1610.

Timoshenko, S.P. and Goodier, J.N., 1982, *Theory of Elasticity,* McGraw Hill Book Co., NY.

Toupin, R. and Bernstein, B., 1961, Sound waves in deformed perfectly elastic materials: Acoustoelastic effect, *J. Acoust. Soc. Am., 64,* 832–837.

Winkler, K.W. and Liu, X., 1996, Measurements of third-order elastic constants in rocks, *J. Acoust. Soc. Am., 100,* 1392–1398.

Winkler, K.W., Sinha, B.K., and Plona, T.J., 1998, Effects of borehole stress concentrations on dipole anisotropy measurements, *Geophysics, 63,* 11–17.

Zhu, Z., Cheng, C.H., and Toksöz, M.N., 1994, Experimental study of the flexural waves in the fractured or cased borehole model, *Expanded Abstracts, Soc. Explor. Geophys.,* 70–73.

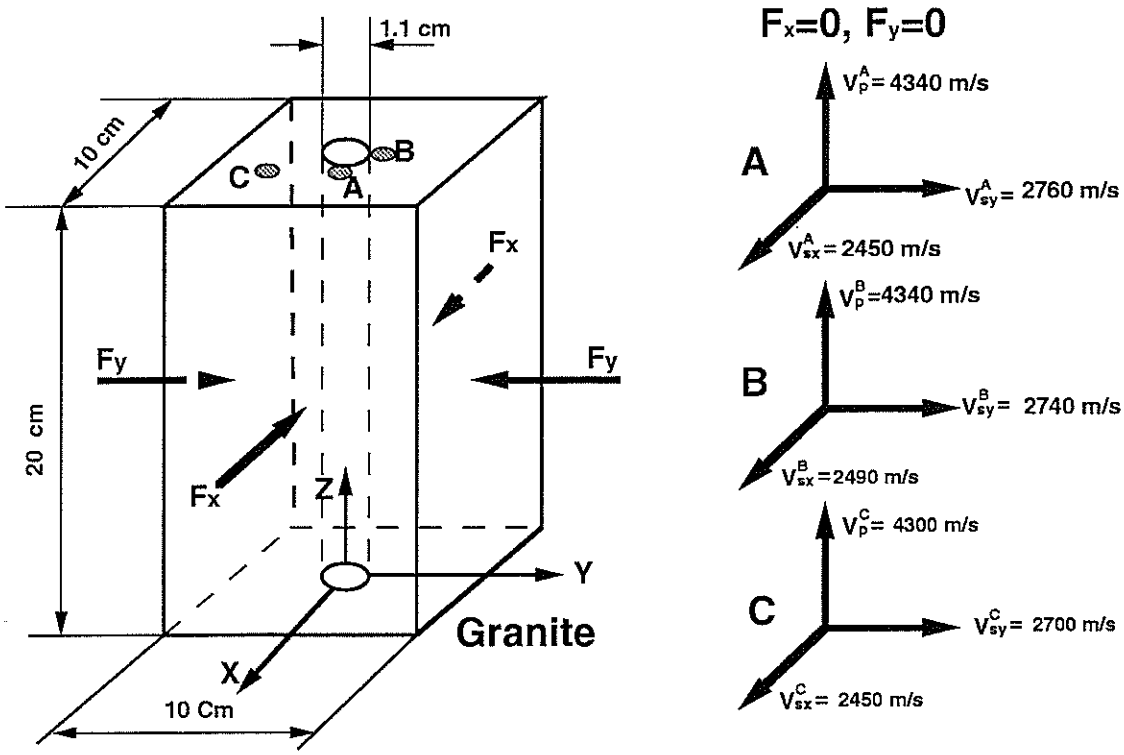


Figure 1: Borehole model. The formation is of orthohombic anisotropy intrinsicly and subject to biaxial stresses in the $x$ and $y$ direction. The diameter of the granite borehole model used in the experiment is 1.1 cm. Footnotes P, Sx and Sy refer to velocities of the P-wave and shear waves polarized in $x$ and $y$ directions, respectively.

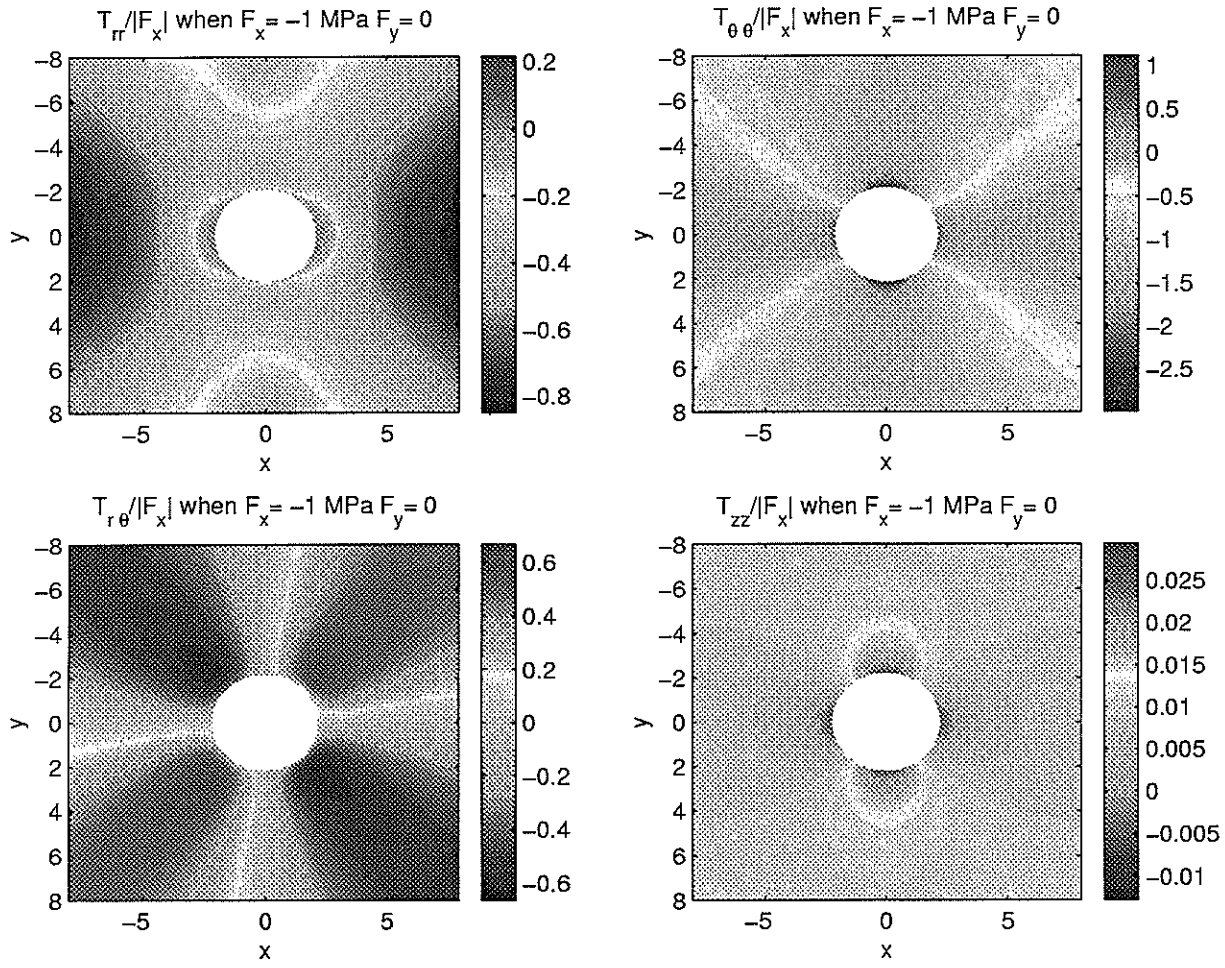


Figure 2: Stress concentration around the borehole induced by compressional uniaxial stress, $F_x = -1MPa$

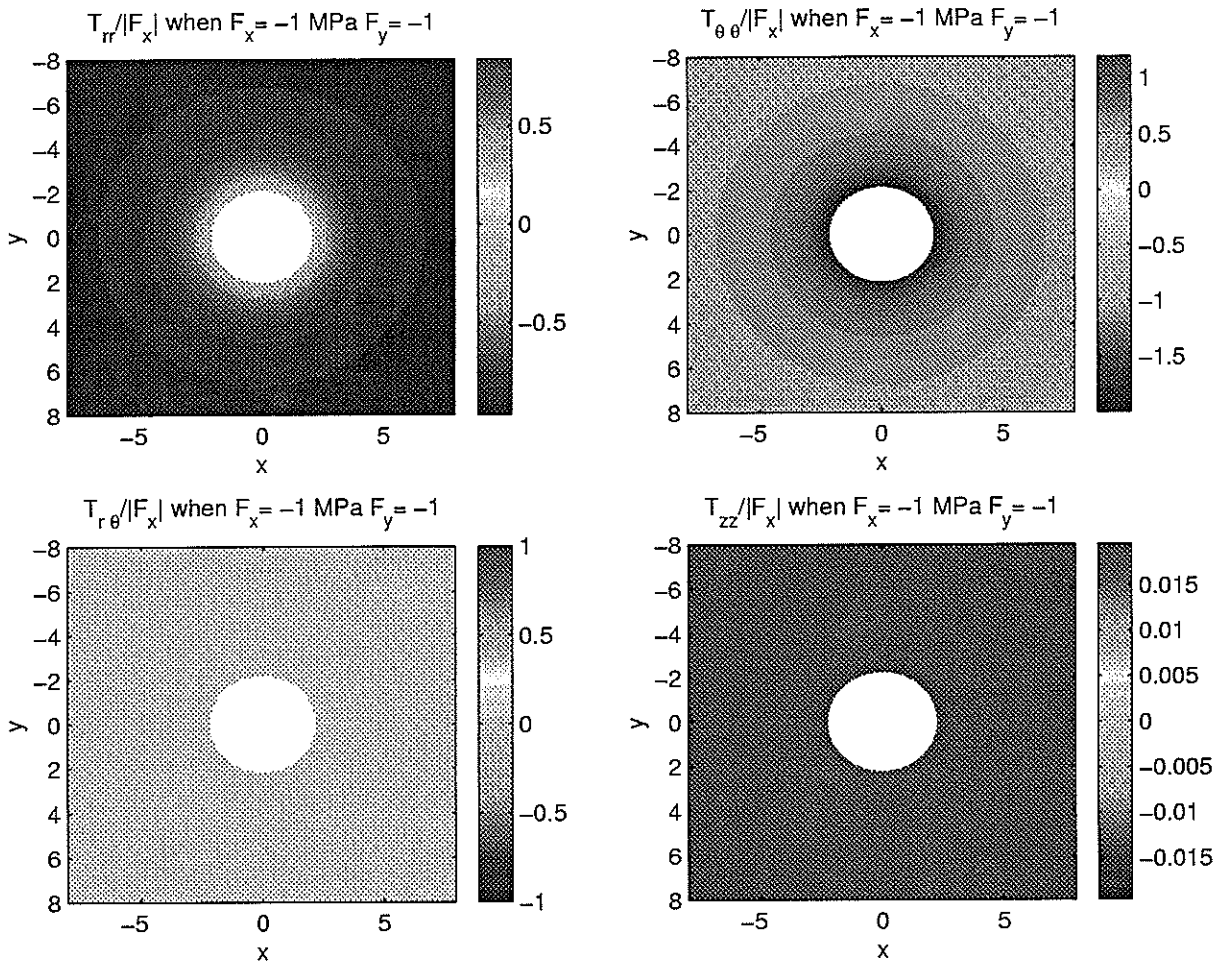


Figure 3: Stress concentration around the borehole induced by biaxial stresses, $F_x = -1MPaF_y = -1MPa$.

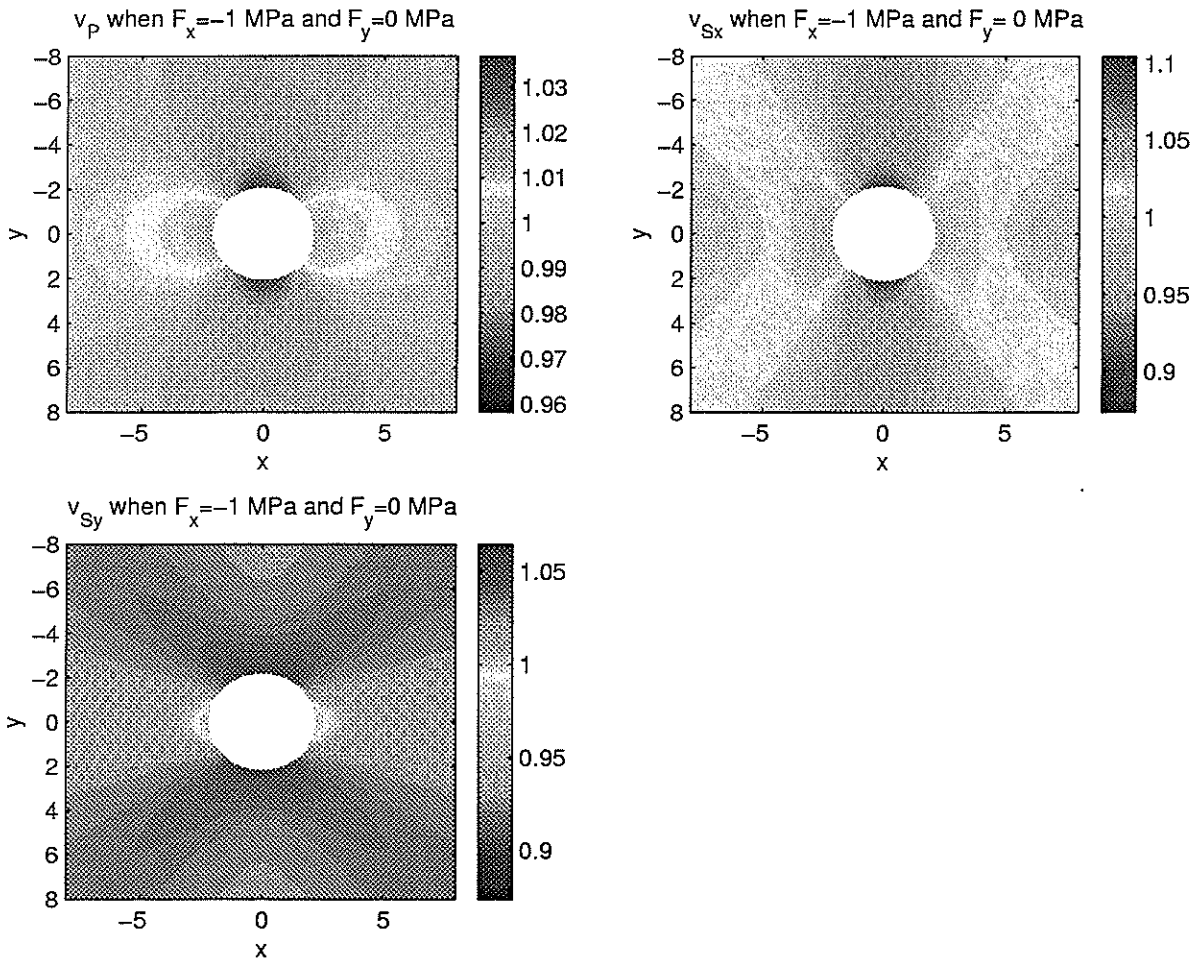


Figure 4: Velocity field in the formation when subject to compressional uniaxial stress, $F_x = -1MPa$.

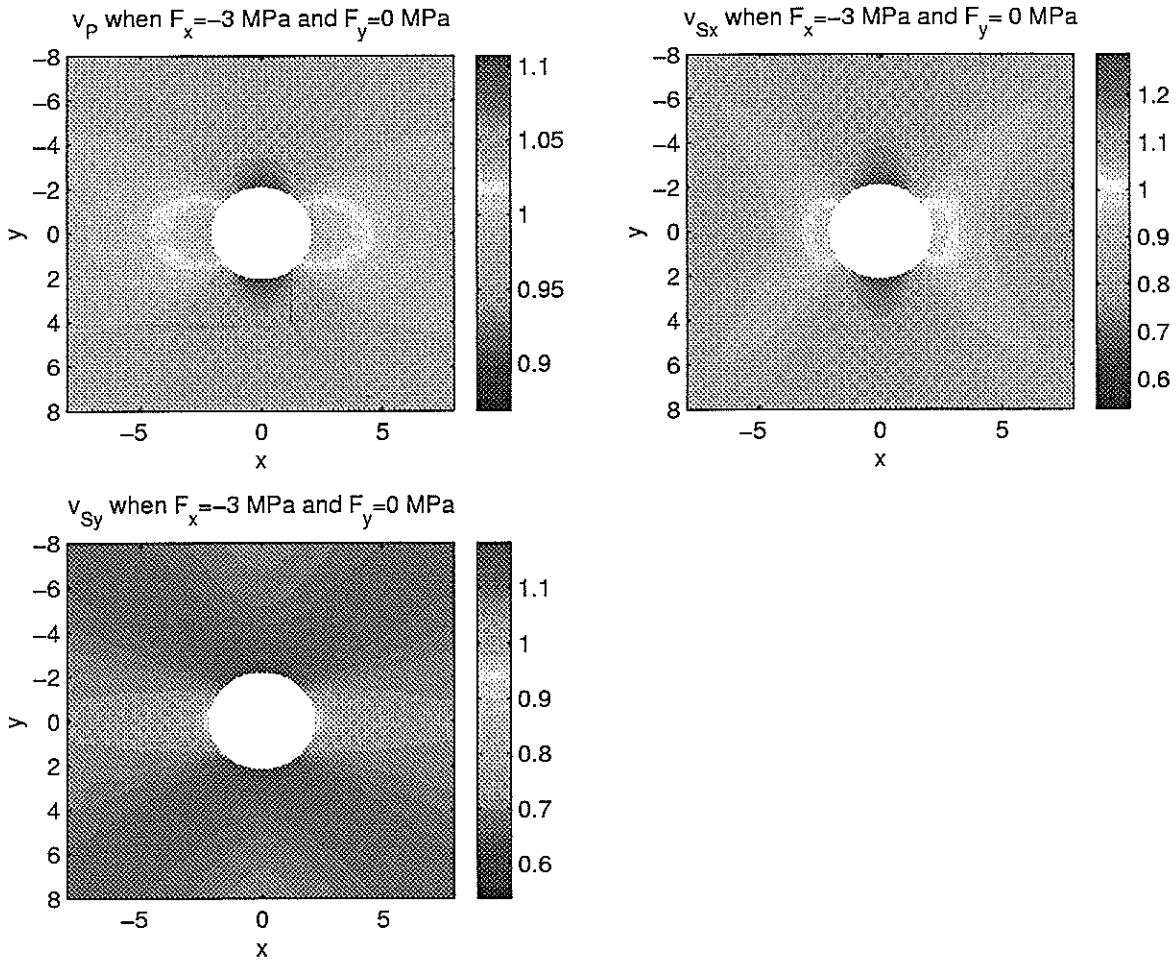


Figure 5: Velocity field in the formation when subject to compressional uniaxial stress, $F_x = -3MPa$.

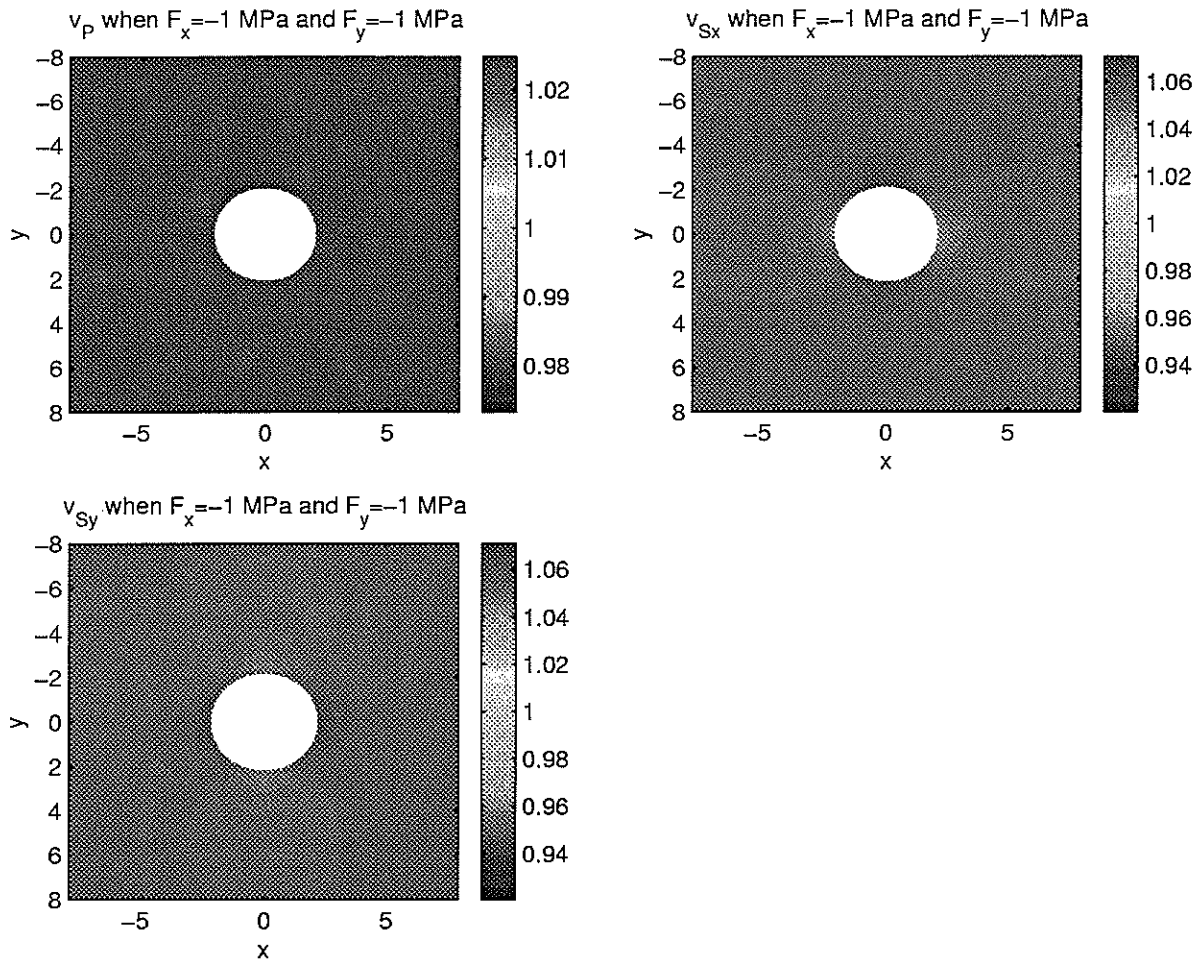


Figure 6: Velocity field in the formation when subject to compressional uniaxial stress, $F_x = F_y = -1MPa$.

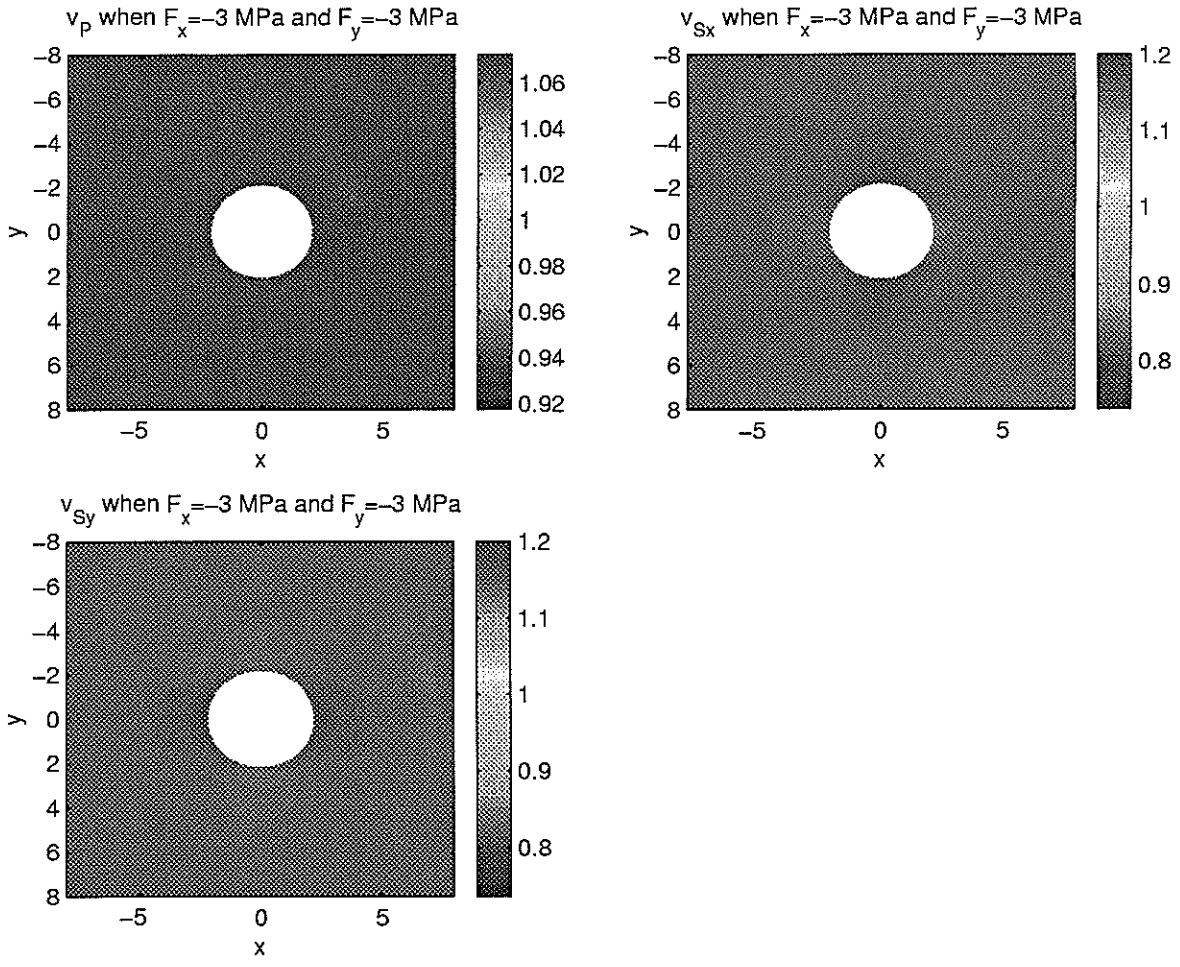


Figure 7: Velocity field in the formation when subject to compressional uniaxial stress, $F_x = F_y = -3MPa$.

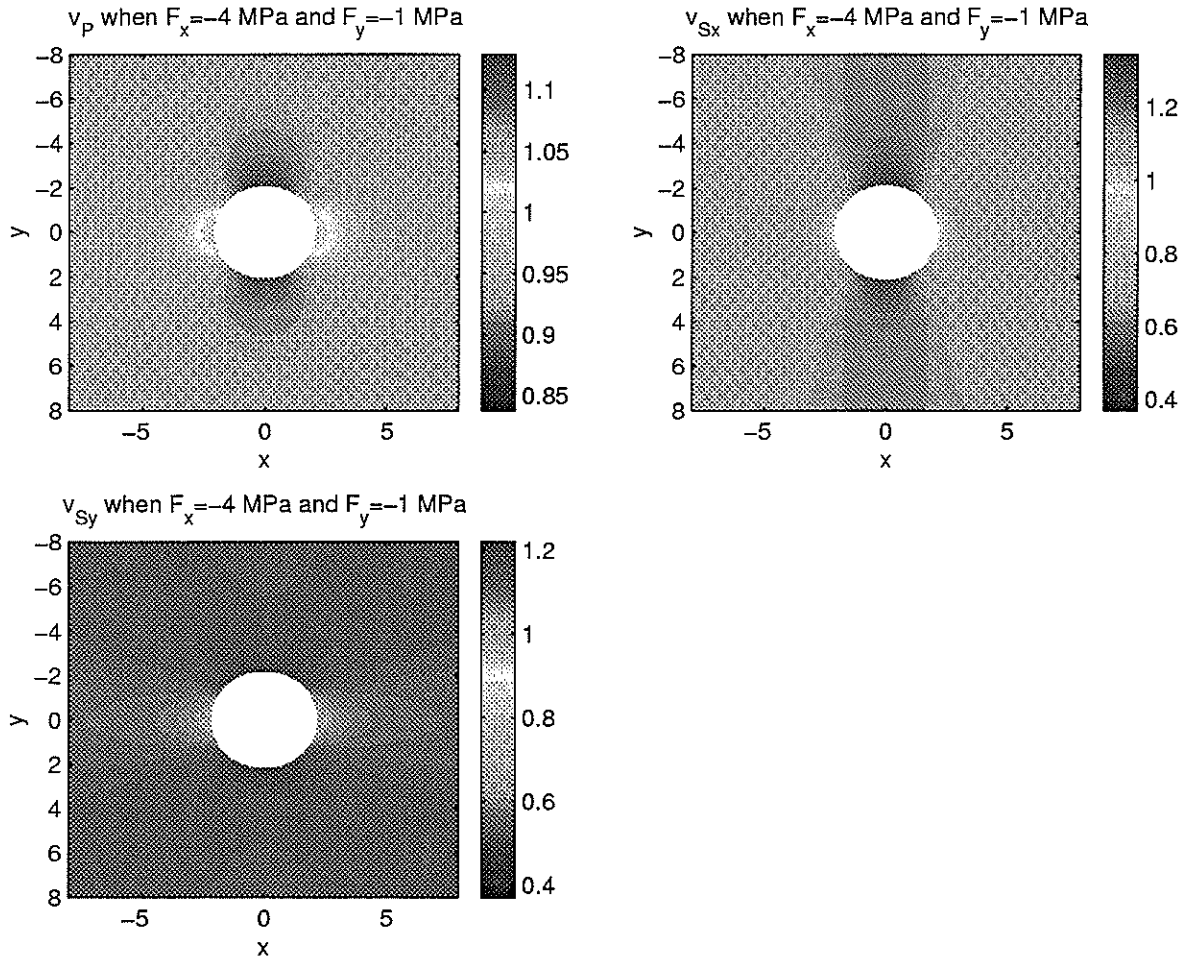


Figure 8: Velocity field in the formation when subject to compressional uniaxial stress, $F_x = -4MPaF_y = -1MPa$.

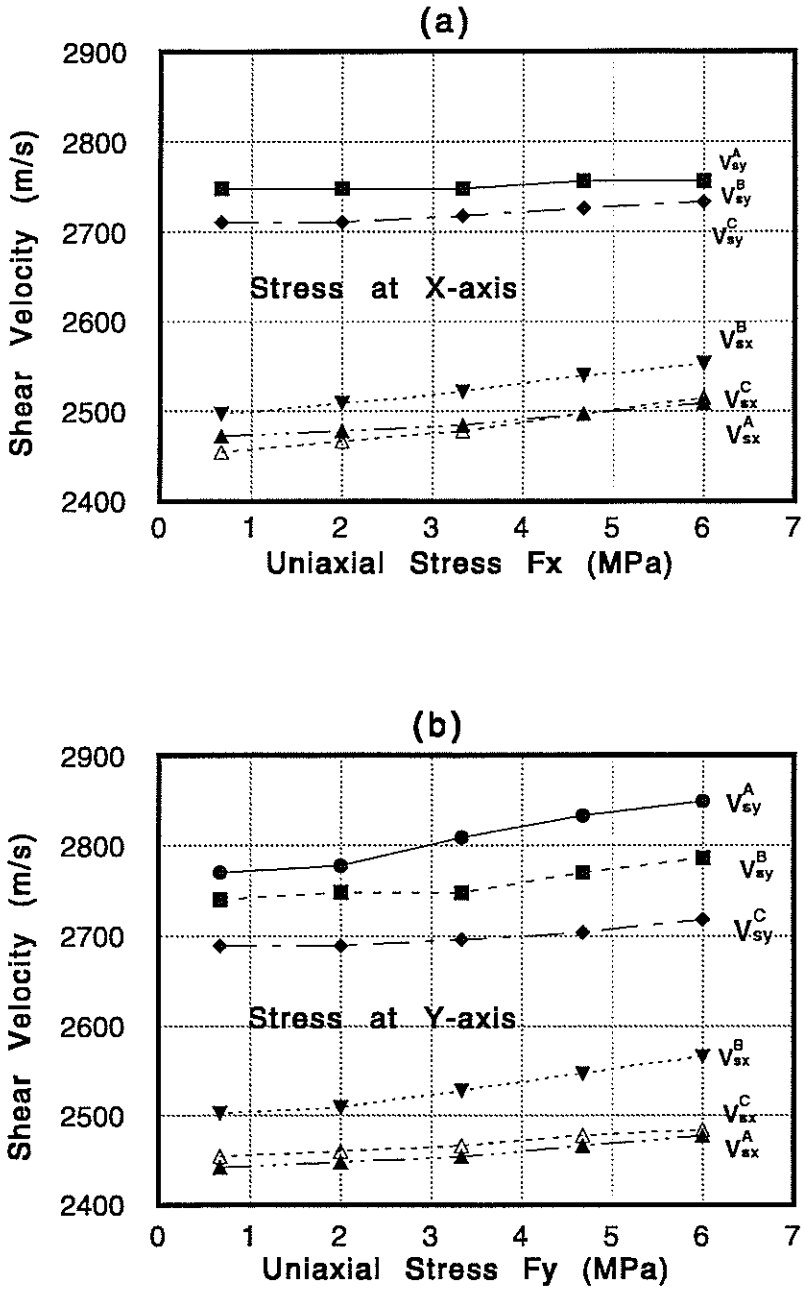


Figure 9: Velocities of fast and slow shear waves when the formation is subject to uniaxial stress in the (a) $x-$ direction, or in the (b) $y-$ direction. Locations (A, B, C) and directions $x$ and $y$ refer to those in Figure 1.

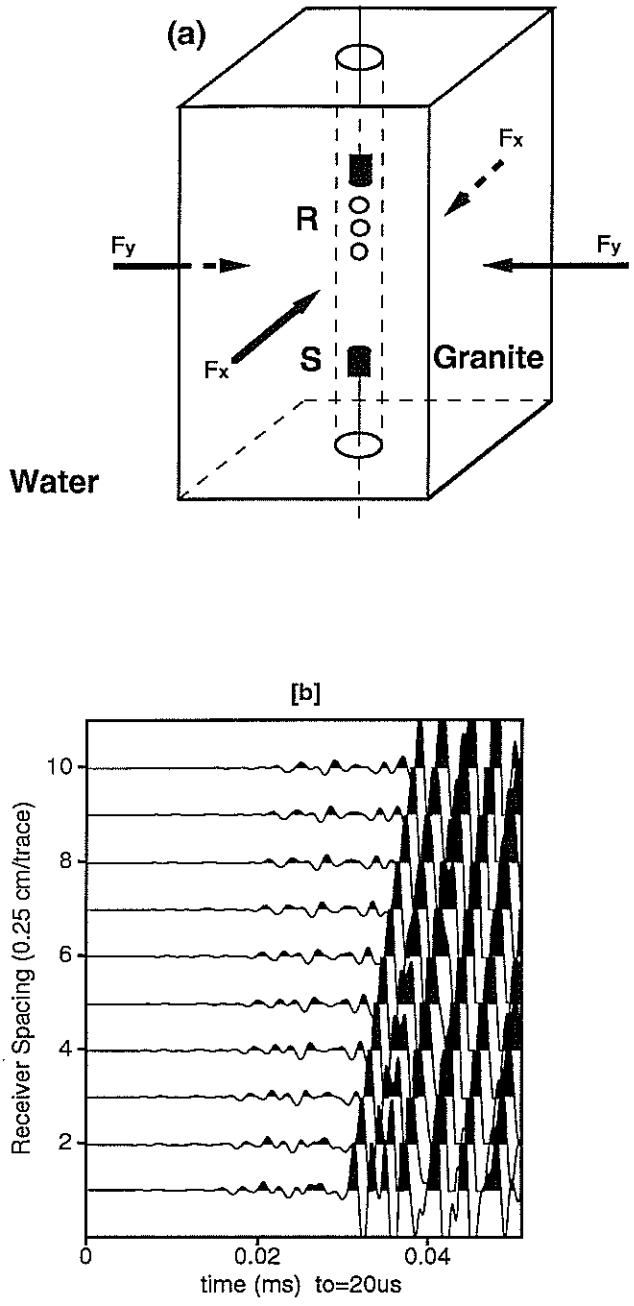


Figure 10: Schematic plot of the experimental setup of (a) monopole logging and (b) typical full waveform record.

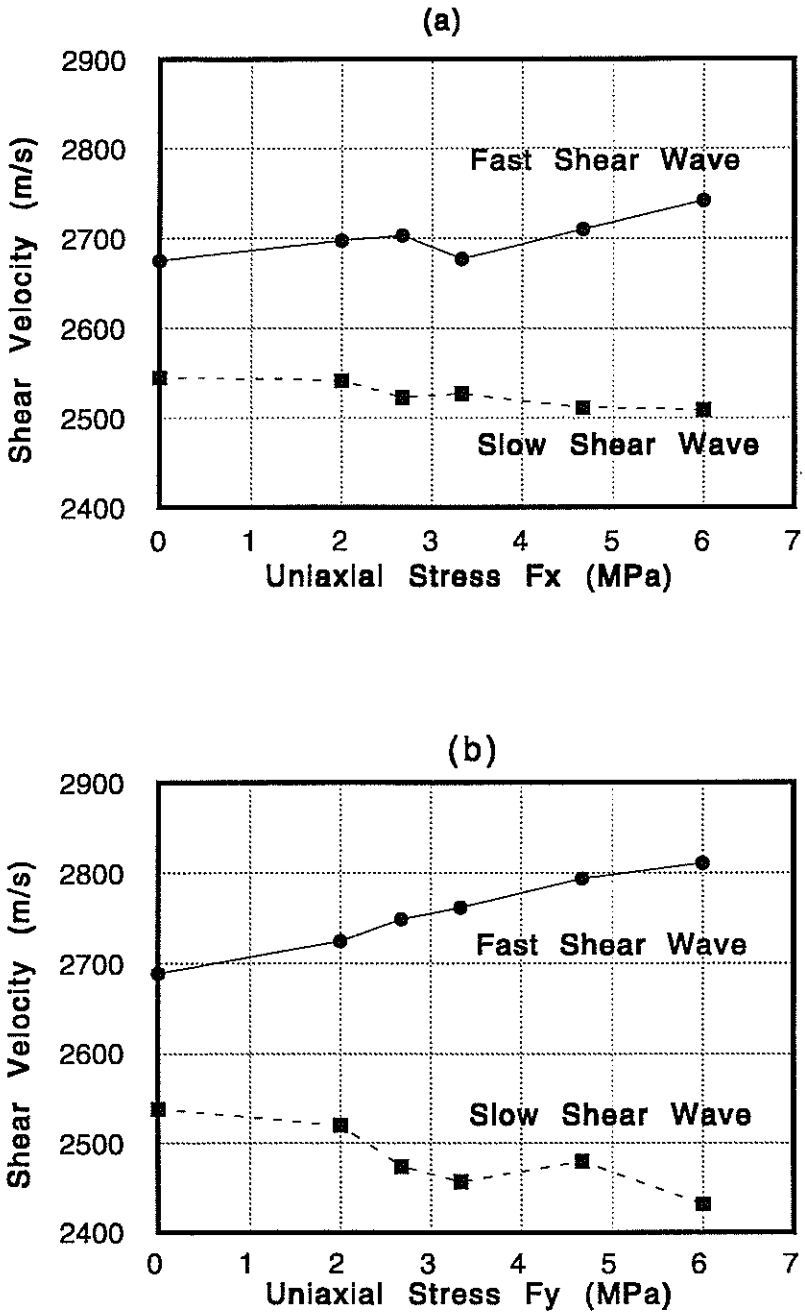


Figure 11: Velocities of fast and slow shear waves measured from monopole logging when the uniaxial stress is in (a) $x$ direction and (b) $y$ direction.